# EXTRACTION OF LAND USE/LAND COVER USING MULTI-TEMPORAL SENTINEL-1A AND LANDSAT INTEGRATION: CASE STUDY OF HANOI

Le Minh Hang (1), Vu Van Truong (1), Tran Van Anh (2)

[1]Insitute of Techniques for Special Engineering, Le Quy Don Technical University,
236 Hoang Quoc Viet, Hanoi, Vietnam
[2] Faculty of Geomatics and Land Administration, Hanoi University of Mining and Geology,
No.18, Pho Vien Street, Duc Thang Ward, Bac Tu Liem District, Hanoi, Vietnam
Email: leminhhang81@gmail.com; truongvv@mta.edu.vn;
tranvananh@humg.edu.vn

**KEY WORDS:** LULC, Sentinel-1A, Landsat, decision tree classification, data fusion

**ABSTRACT:** Satellite images is the major source for classification of land-use/land-cover (LULC). For optical satellite images, the classification is usually based on the spectral reflectance characteristics of the objects. However, optical data is affected by clouds and weather conditions. Radar remote sensing data is less affected by weather conditions but the information on SAR images is only backscatter of roughness of objects. Integration of Sentinel-1A and Landsat data has the main advantages of combining the all-weather capability of the radar sensor, rich spectral information in the visible-near infrared spectrum, with the short revisit period of both satellites. In this paper, a method of integrating multi-temporal Sentinel-1A data and Landsat data were proposed to classify LULC mapping. Normalized difference vegetation index (NDVI), a Normalized Difference Water Index (NDWI) and Enhanced Built-Up and Bareness Index (EBBI) were combinated with the standard deviation, the average of backscatter value of multi-temporal Sentinel-1A and phenology of double-cropped rice. A case study was Hanoi, Vietnam with data included 12 scences of Sentinel-1A, single-polarization VV, Interferometric Wide Swath mode (IW) and GRDH level acquired from Dec 2014 to Nov 2015 and 1 scence of Landsat 8OLI in May 2015. The integrated dataset was classified with Decision tree classification method, which showed the overall classification accuracy of 87%.

## 1. INTRODUCTION

Land cover data tells us how many areas are s covered by forests, wetlands, impervious surfaces, agriculture, and other land and water types. Water types include wetlands or open water. Land use shows how people use the landscape. The different types of land cover can be managed or used quite differently. Land cover can be determined by satellite and aerial imagery analysis, but land use is not... The majority of land use is classified by field surveying or current land use maps. Land cover maps provide information to help managers best understand the current landscape. To see change over time, land cover maps for several different years are needed. With this information, managers can evaluate past management decisions as well as gain insight into the possible effects of their current decisions before they are implemented.

Optical satellite imagery plays an important part in mapping land cover. Recognition of the land cover is based on spectral reflectance characteristics of land cover categories or time series of NDVI indices. However, optical imagery has many disadvantages due to weather condition and cloudiness, especially in the tropical region including Vietnam. The highest expectancy of cloud-free observation could be just one or two times per year only. It is difficult to extract land use/land cover objects, particularly cultivated land if we use only one or two observations. Therefore, agricultural cultivation with harvest interval of three months cannot be detected sufficiently using such infrequent optical imagery.

In recent years, microwave remote sensing technology has been intensively used for monitoring natural resources. Many studies have indicated the correlation between radar backscatter and the different land use such as evergreen forest, deciduous forest, paddy rice, cultivated land… The Sentinel-1A, a European radar imaging satellite, was launched in 2014. The satellite was developed for the specific needs of the Copernicus program in collaboration of European Commission (EC) and European Space Agency (ESA). Sentinel-1A satellite provides SAR images with C-band. The system operates in four observation modes offering medium and high spatial resolution data (up to 5 m) in a swath up to 400 km. Sentinel-1A data has two polarizations such as VV and VH and repeated observation cycle of 12 days. The data is public free. A research from Hang Le Minh proposed to use multi-temporal Sentinel-1A for land cover mapping with accuracy archived 85%. (Hang Le Minh et al, 2017).. The result accuracy was affected by reflection of slope mountain in SAR image. S. Abdikan classified land cover by using dual polarization Sentinel-1A (S.Abdikan et al, 2016). The Support Vector Machines (SVM) method was implemented as a supervised pixel based image classification to classify this dataset that archived 93.28% of overall accuracy. Mary Lum Fonteh compared the classification result by Sentinel-1A and Landsat 8 using SVM classification method (Mary Lum Fonteh et al, 2016). The accuracy by Sentinel-1A was 67.65% and by Landsat was 88.7% . These studies proved the integration of Sentinel-1 and optical satellite image to increase the accuracy. Fusion Sentinel-1 and Landsat data were showed no

significant differences in overall accuracy assessment (88.71% and 88.59%, respectively). Miguel G. Castro Gómez proved using Sentinel-1, Sentinel-2 and vegetation indices by the pixel based to approach with the highest accuracy 84% (Gomez, 2017). The Sentinel-1 and Sentinel-2 integrated dataset classified with an SVM algorithm produce the most accurate LULC map, showing an overall classification accuracy of 88.75% and a Kappa coefficient of 0.86 (Nicola Clerici, 2017). Besides that, the changes of vegetation, especially cropland, affected to the change of LULC (Richards J.F, 1990). Cultivated land was extracted by characterizing seasonal variations and phenology cereal based on time series satellite data. Multi-temporal satellite data provided baseline data to monitor the length of the growing season, peak greenness, onset of greenness, or land-cover changes which associated with events such as fire, drought, land-use conversion, and climate fluctuation (Abdalla M. Faid, 2012), (Moody A, 2001). The major of time-series satellite data used for determining phenology were optical imagery data.

In this paper, the authors proposed to integrate multi-temporal Sentinel-1A and Landsat 8OLI for LULC mapping. Backscatter signal of multi-temporal Sentinel-1A and NDVI, NDWI, EBBI index of Landsat was combined to extract rice crops, built-up land, forest, barren land, shrubs, wetland… The spectral indexes of optical data were used to recognize land cover objects. Based on these land cover objects, land use patterns were classified by time-series SAR data.

## 2. STUDY AREA AND DATA PROCESSING

### 2.1. Study area

Hanoi is located between 20°53' to 21°23' North latitude and 105°44' to 106°02' East longitude, next to Thai Nguyen province, Vinh Phuc province in the North; Ha Nam province and Hoa Binh in the South; Bac Giang province, Bac Ninh province and Hung Yen province in the East; and Hoa Binh province and Phu Tho province in the West (Figure 1a). The Red River is a main river in Hanoi. Its section flowing through Hanoi from Dong Anh district to Thanh Tri district is 40 km long. Hanoi has many waterways, which, although smaller and shorter, are connected with the long-standing history of Hanoi.

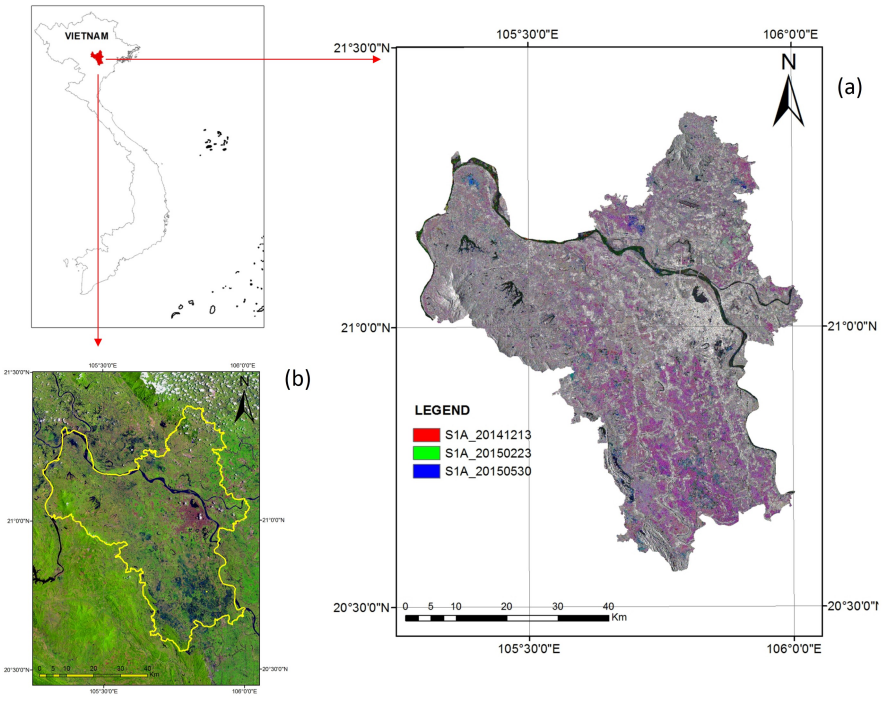


Figure 1. Location of study area; (a) The combination RGB image of three-times Sentinel-1A images; (b) Landsat 8OLI (SWIR-1:NIR:RED)

The majority of the Ha Noi area is situated in the Viet Nam's Red River delta with an average elevation of 5m to 20m above sea level. The hilly areas are in the north and northwest of Soc Son district of the southern edge of Tam Dao Mountains with elevations from 20m to over 400m. The topography of Ha Noi decreases height from north to south and from west to east. The main topographic form is the high alluvial terraces interspersed with low lying lakes. The Hanoi climate is typical for a tropical monsoon climate of the northern climate (hot in the summer, rainy and cold winter, less rainy). With location among tropical zone, Hanoi areas get abundant of solar radiation and high temperatures around the year. The amount of total radiation averages 11,8 kcal/cm$^2$ and year average temperature is 23,6°C. Due to the influence of the East Sea, Hanoi temperature is quite high humidity and rainfall. The average annual humidity is around 79% a year and rainfall is 1,800 mm. There are approximately 114 days

raining a year here.

According to, the LULC objects of Hanoi included in built-up land, barren land, water, wetland, forest, perennial, double-cropped rice, cultivated land, shrubs. In recent years, Hanoi has a rapid urbanization rate, around 3.5 % a year. The increasingly urbanization affected to change LULC objects. The area of cultivated land were decreased and changed to barren land or shrubs. Therefore, updated real-time the changes of LULC by remote sensing data is important to monitor and plan for using land of Hanoi.

### 2.2. Data material and pre-processing

In this study, Sentinel-1A data in observation Interferometry Wide Swath (IW) mode acquisition from December 2014 through November 2015 were used (Figure 1b). We used Level-1.5 Ground Range Detected (GRD) products. This level consist of focused SAR data that has been detected, multi-looked and projected to ground range using an Earth ellipsoid model such as WGS84. The terrain height used varies in azimuth but is constant in range (ESA, n.d.). Landsat 8 data was acquired at 30/05/2015 with Level-1 (Geotiff) (Figure 1c). Details of the characteristics of the data materials are shown in Table 1.

**Table 1. Multi-temporal Sentinel-1A and Landsat 8OLI**

| | Landsat 8OLI/TIRS | Sentinel-1A |
|---|---|---|
| **Acquisition time** | 30/05/2015 | 13/12/2014;30/01/2015;23/02/2015;<br>19/03/2015;12/04/2015;30/05/2015;<br>23/06/2015;17/07/2015;19/08/2015;<br>03/09/2015;21/10/2015;14/11/2015; |
| **Acquistion orbit** | 127/45 and 127/46 | Ascending |
| **Data product** | Level – 1 | Interferometric Wide (IW) – GRDH |
| **Polarization** | | VV-polarization |
| **Imaging frequency** | Blue; Green; Red; NIR; SWIR-1;SWIR-2 | C-band (5.46 Hz) |
| **Resolution** | 30m | 10m |
| **Bit depth** | 16 bit | 16 bit |

Sentinel-1A data were pre-processed using the open source software SNAP Toolbox of European Space Agency. Pre-processing of SAR image consisted of geocoding, radiometric calibration, incidence angle normalization. The geocoding step involved a Range Doppler Terrain correction processing that used the elevation data from the 1 arc-second DEM product from the Shuttle Radar Topography Mission (SRTM) provided by ESA. In this process, data are resampled and geo-coded to a grid of 10m spacing to preserve the 20mx5m spatial resolution according to the NY Quist sampling thermo (Daniel Sabel, 2012). The data pre-processing in this study has been performed in four main steps such as (1) Resampled and geo-coded by DEM product; (2) Backscatter normalization to sigma-nought ($\sigma^0$) of intensity band; (3) Convert linear to/from dB; (4) Multi-temporal Speckle filter.

In otherwise, Landsat 8 data were converted to TOA reflectance by Envi 5.2 software. The formula TOA reflectance of Landsat 8 are shown on USGS website (USGS, n.d.).

### 2.3. Field Survey data

A field survey was conducted by using the Locus map which is an application software on Android system. Locus map is capable of locating points by GPS and taking photos. A distance of 40 km was covered the study area during the survey and around 100 ground truth points were collected. The ground truth points include LULC objects, cultivated land and rice fields.

## 3. METHODOLOGY

### 3.1. Analysis characteristics of LULC

LULC have different characteristics of spectral reflectance and backscatter value. According to multi-temporal SAR images, there are two main objects such as changed/unchanged objects which considered in a one-year cycle. Unchanged objects are built-up land, forestry land, perennial, lake, river, barren land. Many backscatter signal at lake or river was created by the movement of vehicles on the water surface which changed the surface at the time signals being received. Forestry patterns in Hanoi are mainly evergreen forest, canopy density therefore unchanged over time. The changed objects are wetland, cultivated land, rice crops. The analysis characteristics of LULC objects by multi-temporal Sentinel-1A images are shown on Figure 2.

Figure 2 shows the backscatter value of LULC objects in time series Sentinel-1A datain which backscatter value of the unchanged objects such as urban, rural, forest/perennial, urban greeness, shrub/fallow, barren and water have the similar backscatter value in period of time. Rural and urban have the highest backscatter value. Besides, Forest/perennial, urban greenness and shrub/fallow have similarity backscatter value. According to Figure 2a and Figure 2b, water and barren (which have the smooth surface) have the lowest backscatter value. In other hands, the changed objects such as cultivated land, rice crop and wetland have the different backscatter signal base on

characteristic of these at the acquired time. There were big changes of wetland objects in Western Hanoi due to the water surface areas were used for farming or other purposes. The backscatter value of cultivated land or rice crop were changed by phenology of vegetations or hybrid rice (Figure 3 and Figure 4).

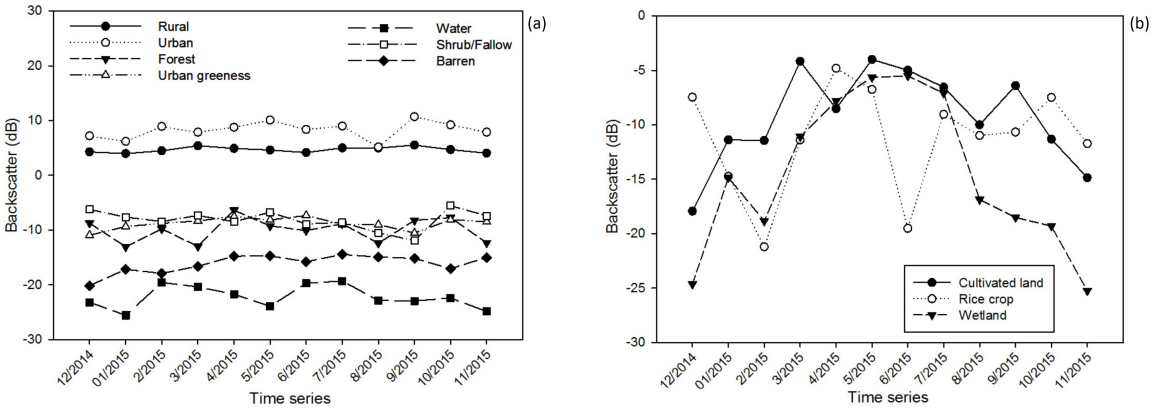


Figure 2. (a) Backscatter signal (dB) of unchanged object; (b) Backscatter signal (dB) of changed object

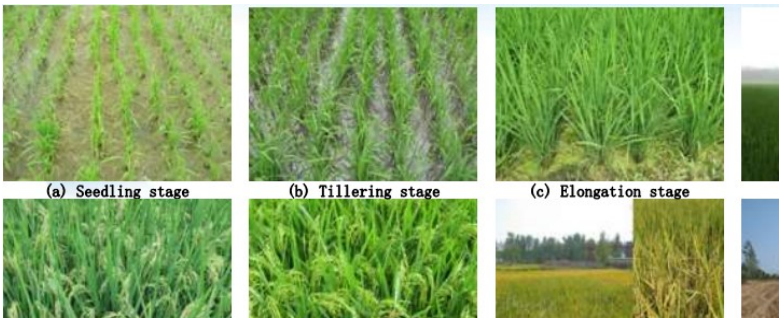


Figure 3. Rice phenology (Hybrid rice)

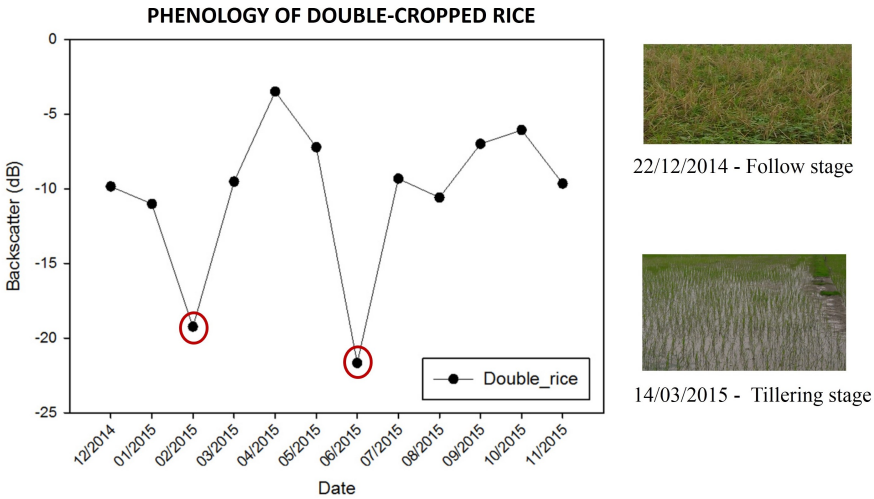


Figure 4. Phenology of double-cropped Rice in Sentinel-1A data

According to field survey in paddy rice area of Hanoi, cultivated lands are mainly used for growing rice from January to June and from July to October. In the others period, these lands were abandoned or used for growing crops, due to rice cultivation in this period did not bring high economic efficiency. Besides, land cover objects have different spectral characteristic by multispectral satellite image. Figure 5 shows spectral analysis of LULC by optical image.

### 3.2. Proposal method

In this study, the authors proposed a classification method for LULC objects by integrating multi-temporal Sentinel-1A and Landsat 8OLI. As depicted in Figure 5, LULC objects changed or unchanged in the experiment

period. The differences play an important part in identification of LULC objects by standard deviation value. This standard deviation value was determined by Eq (2):

$$std = \left( \frac{1}{n-1} \sum_{i=1}^{n} \left( x_i - \bar{x} \right)^2 \right)^{\frac{1}{2}} \quad (2)$$

where $\bar{x} = \frac{1}{n} \sum_{i=1}^{n} x_i$ is mean backscatter value of multi-temporal pixel; $x_i$ is backscatter value of each pixel at a period image

In addition, standard deviation, mean backscatter value and phenology of rice were used to recognize LULC patterns (Figure 5a, Figure 5b). Double-cropped rice was classified based on the low peaks of backscatter value in time-series Sentinel-1A in February and June in the year (Figure 5c) by using Matlab R2017. Texture images of time series Sentinel-1A are shown in Figure 5a, Figure 5b which included standard deviation image, mean image and double-cropped rice image. To be more precise, LULC objects were classified more clearly than by optical image. In this article, the authors proposed three spectral indices such as Normalized difference vegetation index (NDVI), a Normalized Difference Water Index (NDWI) and Enhanced Built-Up and Bareness Index (EBBI). These spectral indexes were chosen because the confuses were identified only by SAR images, for example, reflection slope of mountains, roughness surfaces, fallow land (which is only grasses and weeds). The spectral index images were automatically classified to the binary image by Otsu's method in Matlab.

According to the advantages of SAR image and optical image, the classification method was decision tree method for LULC mapping. The flowchart-like structure of decision tree and nodes are shown on Figure 8. The threshold of decision nodes were based on standard deviation and mean backscatter value.

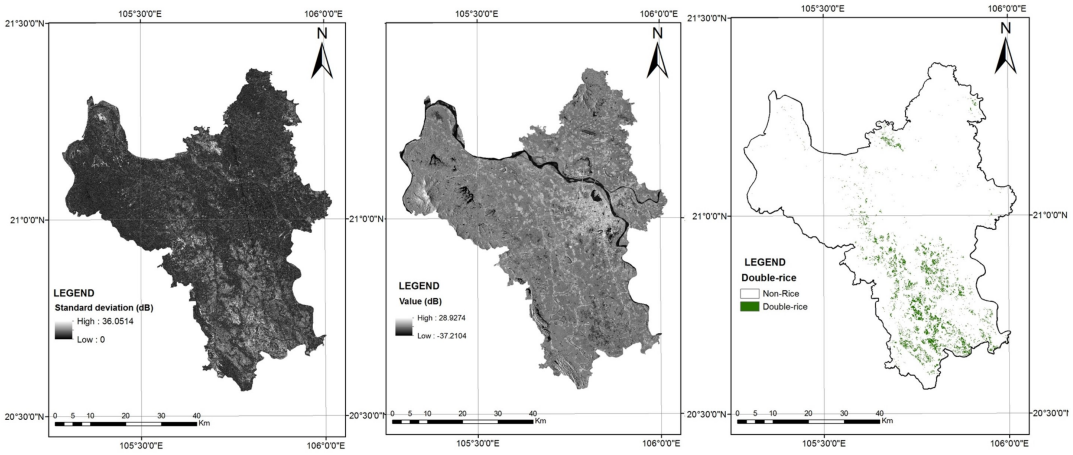


(a) (b) (c)

Figure 5. Texture images by multi-temporal Sentinel-1A; (a) Standard deviation image; (b) Mean value image; (c) Double-rice image

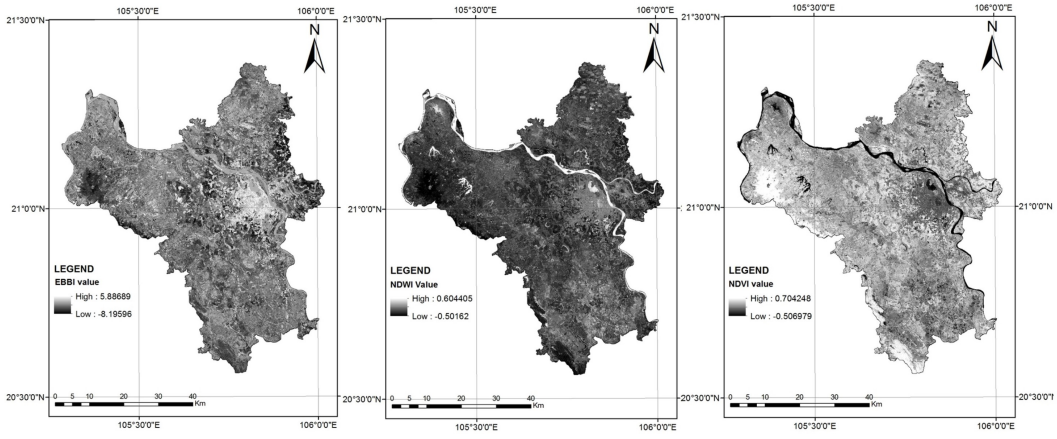


(a) (b) (c)

Figure 6. Spectral index image calculated by Landsat 8OLI such as (a) EBBI; (b) NDWI; (c) NDVI

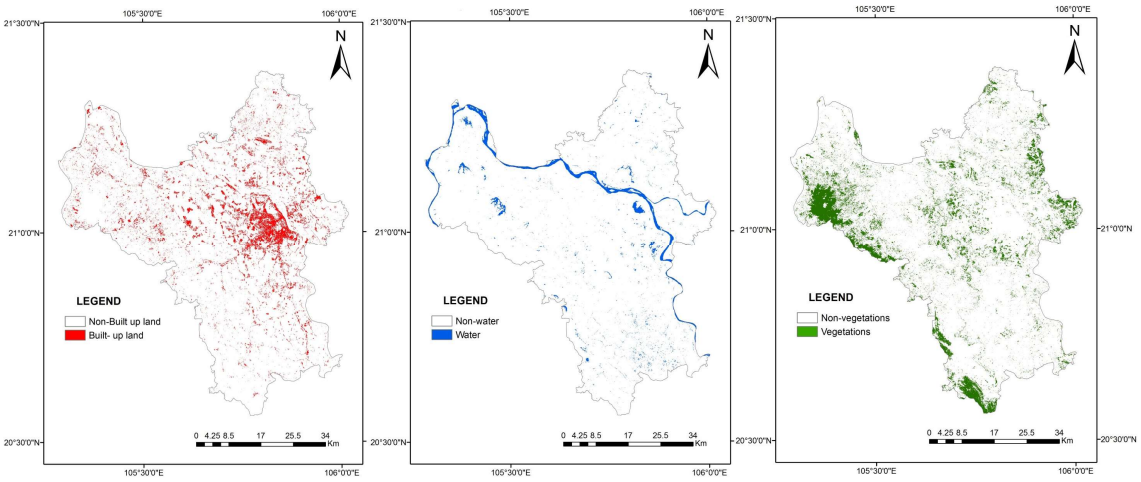


Figure 7. Classified image of spectral index image by Otsu's method

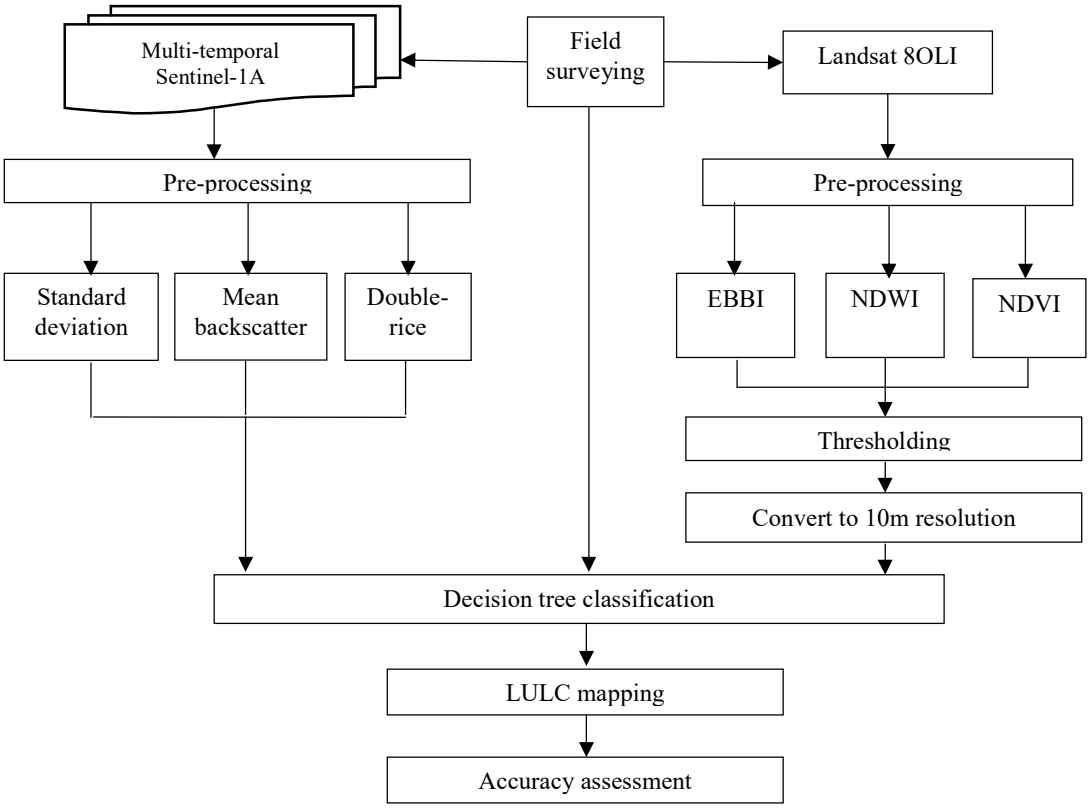


Figure 8. The flowchart of proposal method

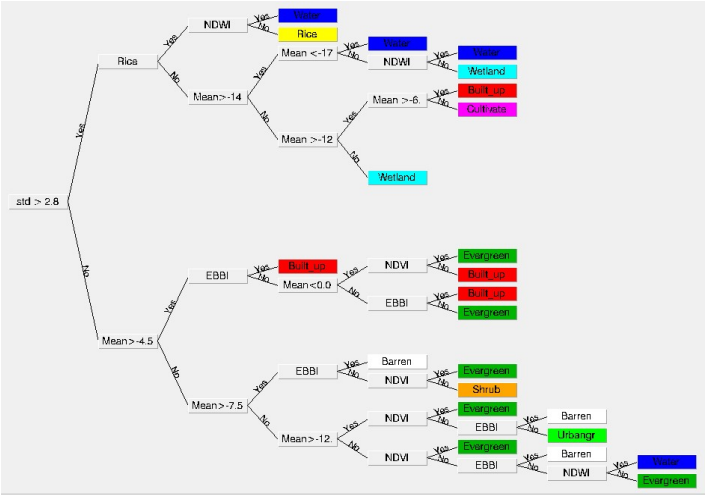


Figure 9. The threshold of decision tree classification

## 4. DISCUSSION AND CONCLUSION

LULC mapping of Hanoi by integrating of multi-temporal Sentinel-1A and Landsat 8OLI is shown in Figure 10. Based on field surveys, LULC objects were chosen as built-up land, double-cropped rice, lake/river (water), wetland, forest/perennial, cultivated land, barren, urban green and shrub/fallow land. The LULC objects were chosen by expert and field surveying.

The accuracy assessment could be clearly identified in both Landsat image, Google Earth and Google Map. A total of 200 points (locations) were automatically created in the classified image of the study area. The accuracy of the proposal method was shown in Table 2. The results from accuracy assessment showed an overall accuracy obtained from the random sampling process is 87.0%..

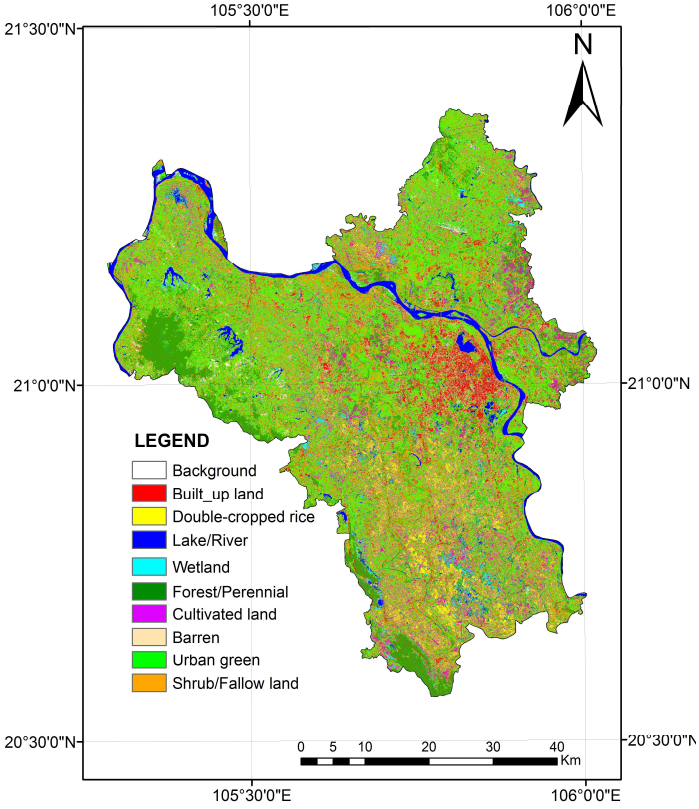


Figure 10. LULC mapping of Hanoi

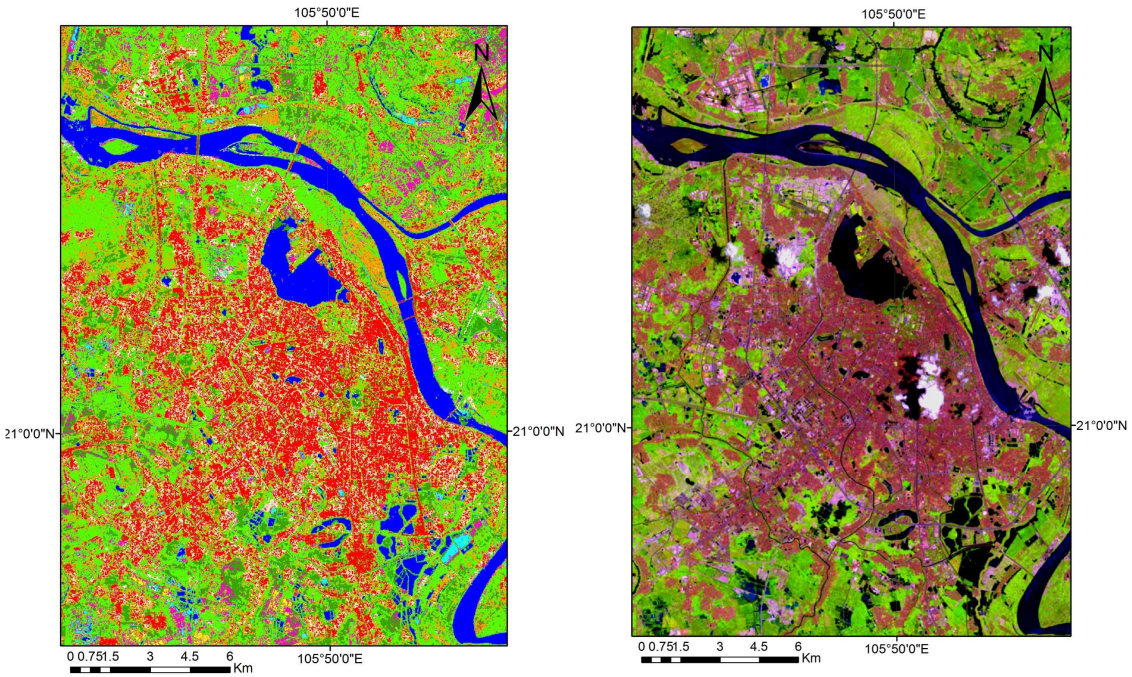


Figure 11. Compare the classification result and RGB combination of Landsat 8OLI at the centre of Hanoi; (a) LULC mapping at the centre of Hanoi; (b) RGB combination of Landsat 8OLI (SWIR:NIR:R)

**Table 2. Accuracy assessment of proposal method**

| | | Reference data | | | | | | | | | Total | UA (%) |
|---|---|---|---|---|---|---|---|---|---|---|---|---|
| | | Water | Wetland | Cultivated | Shrubs | Forest | Urban Green | Barren | Rice | Built-up | | |
| Classification data | Water | 2 | 0 | 0 | 0 | 0 | 0 | 0 | 0 | 0 | **2** | **100** |
| | Wetland | 1 | 2 | 0 | 0 | 0 | 0 | 0 | 0 | 0 | **3** | **67** |
| | Cultivated | 0 | 1 | 22 | 0 | 0 | 0 | 0 | 0 | 0 | **23** | **96** |
| | Shrubs | 0 | 0 | 0 | 61 | 2 | 2 | 0 | 0 | 1 | **66** | **92** |
| | Forest | 0 | 0 | 2 | 0 | 16 | 2 | 0 | 0 | 0 | **20** | **80** |
| | Urban green | 0 | 0 | 3 | 9 | 0 | 41 | 1 | 0 | 0 | **54** | **76** |
| | Barren | 0 | 0 | 0 | 0 | 0 | 0 | 8 | 0 | 0 | **8** | **100** |
| | Rice | 0 | 0 | 0 | 0 | 0 | 1 | 0 | 15 | 0 | **16** | **94** |
| | Built-up | 0 | 0 | 0 | 0 | 0 | 1 | 0 | 0 | 7 | **8** | **88** |
| | **Total** | **3** | **3** | **27** | **70** | **18** | **47** | **9** | **15** | **8** | | |
| **Overall accuracy 87.0%** | | | | | | | | | | | | |
| **Kappa: 0.828** | | | | | | | | | | | | |

According to the table 2, the user's accuracy ranged from 67.1% to 100%. Barren and water (lake/river) patterns had a little of check points and clearly identified in the optical image by spectral indices so that they had the highest accuracy. Urban green was defined by trees which along with the streets and growning around the buildings. As a result, it is difficult to classify urban green by NDVI index and texture of the SAR image. Urban green archived accuracy 76% while it confused with cultivated land and barren land. Rice crops, cultivated land and shrub had higher accuracy than others because of the knowledge of rice phenology and change of cultivated land or unchanged of shrubs based on time-series SAR images. Texture images of multi-temporal SAR images had an important role in the

classification of changed/unchanged patterns and intensity of LULC objects. Spectral index images improved to identify land cover patterns which were confused by SAR image, for example perpendicular reflectance of slope mountain, smoothness surface (airport runway), types of vegetations (rice, cultivated land, shurb, forest, urban green…).

In conclusion, satellite image is very important for the production of land use/land covr mapping which based on a method classification . Using only multi-temporal SAR images can classified some LULC patterns, for example rice crop, forest, built-up, water, wetland, cultivated land. However, there were some confusion at high areas or smoothness surface. Hence, integrating multi-temporal SAR images and optical image increased the number patterns of LULC which were identified by satellite images. Besides, the proposal fusion method increased classification accuracy to 87.0%. The method can help improve the monitoring LULC by remote sensing data.

**REFERENCES**


Abdalla M. Faid, e. (2012). Monitoring land-use change-assosiated land development using multitemporal Landsat data and geoinformatics in Kom Ombo area, South Egypt. *International Journal of Remote Sensing*, 7024-7046.

Bjorn Waske, e. (2009). Classifier ensembles for land cover mapping using multitemporal SAR imagery. *ISPRS Journal of Photogrammetry and Remote Sensing, 64*, 450-457.

Daniel Sabel, e. (2012). Development of a global backscatter model in support to the Sentinel-1 mission design. *Remote Sensing of Environment*, 102-112.

ESA. (n.d.). Retrieved from https://earth.esa.int/web/sentinel/user-guides/sentinel-1-sar

Gomez, M. G. (2017). *Joint use of Sentinel-1 and Sentinel-2 for land cover classification: A machine learning approach.* Lund University GEM thesis series nr 18: Department of Physical Geography and Ecosystem.

Hang Le Minh, e. (2017). Mapping land cover using multi-temporal Sentinel-1A data: Acase study in Hanoi. *Vietnam journal of earth sciences*, 345-359.

Lopez, C. V. (2017). Fusion of very high resolution SAR and optical images for the monitoring of urban areas. *IEEE*.

Mary Lum Fonteh, e. (2016). Assessing the utility of Sentinel-1 C band Synthetic Aperture Radar imagery for land use land cover classification in the tropical coastal systems when compared with Landsat 8. *Journal of Geographic information system*, 495-505.

Moody A, e. (2001). Land-surface phenologies from AVHRR using the discrete Fourier transform. *Remote sensing environment*, 305-323.

Myneni, R. e. (1995). The interpretatin of spectral vegetation indexes. *IEEE Trans. Geosci. Remote Sensing*, 481-486.

Nicola Clerici, e. (2017). Fusion of Sentinel-1A and Sentinel-2A data for land cover mapping: A case study in the lower Magdalena region Colombia. *Journal of Maps, Taylor & Francis Online*.

Richards J.F, e. (1990). *Land transformations. In the Earth as transformed by human action: Global change and regional changes in the Biosphere over the past 300 years.* New York, USA: Cambridge University Press.

S.Abdikan, e. (2016). Land cover mapping using Sentinel-1 SAR data. *The International Archives of the Photogrammetry, Remote Sensing and spatial information sciences. XLI-B7.* Prague, Czech Republic: XXIII ISPRS Congress.

Tucker C.J, e. (1985). African land-cover classification using satellite data. *Science*, 369-375.

USGS. (n.d.). Retrieved from https://landsat.usgs.gov/using-usgs-landsat-8-product

X.Wen, C.Li . (2012). Feature-level image fusion for SAR and optical images. *IET International Conference on Information Science and Control Engineering* .